Liu *et al. Biochar* (2025) 7:69
https://doi.org/10.1007/s42773-025-00460-4

Biochar

ORIGINAL RESEARCH Open Access

Does biochar field aging reduce the kinetic retention for weakly hydrophobic antibiotics in purple soil?

Xinyu Liu[1,2], Yang He[1,3,4*], Jinghan Li[1], Jiahui Li[1], Jianqiang Zhang[1] and Xiangyu Tang[2,5]

Abstract

The impact of field aged biochar (FABC) on the adsorption kinetics and transport behavior of weakly hydrophobic antibiotics in soil is scarcely discussed. This study investigated the impact of FABC on weakly hydrophobic antibiotics (sulfadiazine, SD and florfenicol, FF) transport in purple soil by comparing fresh biochar (FBC), one-year aged biochar (ABC1), and five-year aged biochar (ABC5). Through batch adsorption, soil column experiments, and Hydrus 1D modeling, this study examined the evolution of physicochemical properties of biochar, their effects on soil porosity and dispersion, and antibiotic adsorption. Results showed that aging significantly altered biochar characteristics, with carbon (C) content decreasing by 10.40% while oxygen (O) content increased by 40.52%. ABC1 demonstrated optimal performance with a 99.28% increase in specific surface area (SSA) and enhanced oxygen-containing functional groups, leading to maximum antibiotic retention rates of 16.57% for SD and 24.78% for FF. Although ABC5 showed decreased SSA and adsorption capacity, it maintained stable remediation effects through enhanced biochar–soil interactions, as evidenced by increased dispersivity (λ) and hydrodynamic dispersion coefficient (D). The two-site chemical nonequilibrium model (TSM) revealed that the fraction of equilibrium adsorption sites (f) increased from 0.1164 to 0.3514 after aging, indicating improved antibiotic retention. These findings demonstrate that while one-year aging enhanced remediation capacity, five-year aging stabilized environmental effects through modified soil structure.

Article Highlights

- One-year aged biochar showed optimal antibiotic retention through enhanced specific surface area and functional groups, while five-year aging stabilized remediation effects despite reduced adsorption capacity.
- Aging of biochar progressively changed soil water transport patterns and soil-biochar interactions.
- Antibiotic transport in aged biochar shifted from adsorption-dominated to dispersion-influenced mechanisms.

Keywords Field aging, Biochar, Antibiotics, Adsorption, Dispersivity, Soil

*Correspondence:
Yang He
yanghe@swjtu.edu.cn
Full list of author information is available at the end of the article

Graphical Abstract

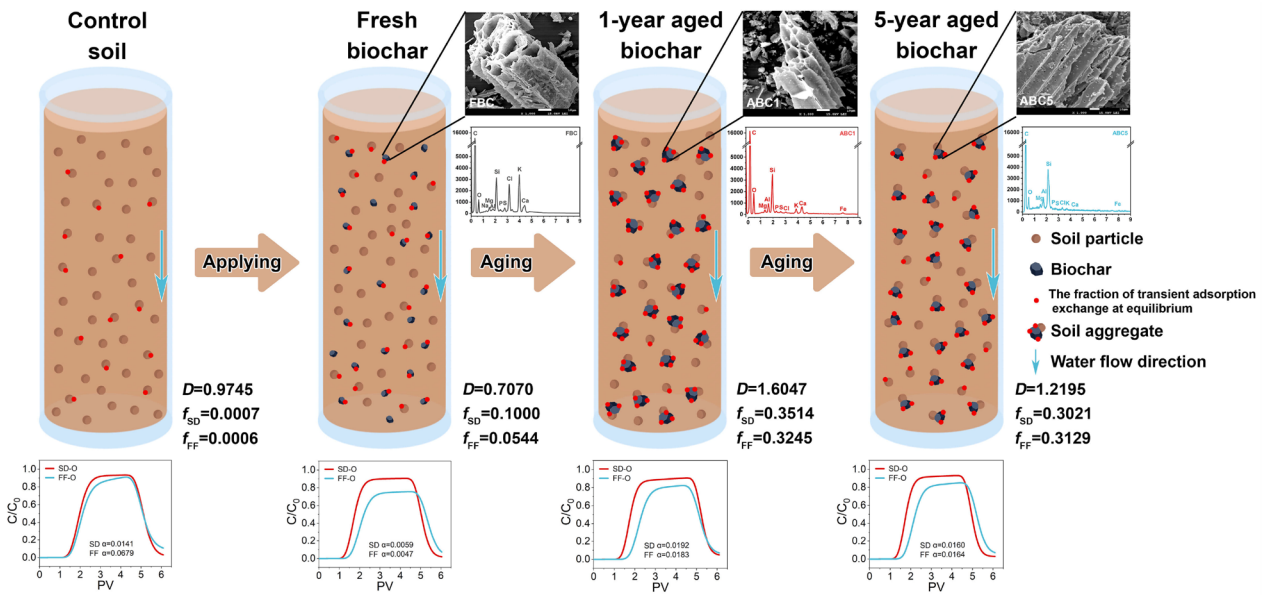

1 Introduction

Biochar has emerged as a promising soil amendment that significantly enhances soil fertility and facilitates contaminated soil remediation (Wang et al. 2020). Its pollutant adsorption capacity exceeds that of soil organic matter by an order of magnitude (Kong et al. 2014). Nevertheless, the aging process of biochar is inevitable, and the resulting changes in surface characteristics show significant differences between field conditions and laboratory-simulated aging (Wang et al. 2020). In this regard, studies have demonstrated that adsorption capacity of biochar initially increases and then decreases during aging compared to fresh biochar (FBC) (Martin et al. 2012; Ren et al. 2018). Specifically, the aging process results in substantial dissolved organic carbon (DOC) emissions and changes in specific surface area (SSA), accompanied by increased carbon (C), nitrogen (N), and oxygen (O) ratios (Tan et al. 2019). These modifications enhance the formation of oxygen-containing functional groups (Mia et al. 2017) and surface hydrophilicity (Zimmerman 2010).

The effects of biochar aging on soil adsorption remain controversial. Batch experiments showed that aging decreased the Freundlich coefficient (K_f) for sulfadiazine (SD) from 12.65 to 9.17 (Yin et al. 2019) and for florfenicol (FF) from 351.43 to 224.75 $\mu g^{1-1/n}$ $(cm^3)^{1/n}$ g^{-1} (He et al. 2019). Conversely, some studies reported enhanced retention after aging, with 1.4–16.3 times higher adsorption coefficients (K_d) (Lei et al. 2020; Li et al. 2020). Similarly, Tang et al. (2024) observed 2.8 to 10.1 times higher K_f values in field-aged biochar (FABC) compared to FBC. Biochar application significantly alters soil hydraulic properties, increasing saturated conductivity by 25% and water holding capacity by 15% (Omondi et al. 2016). Moreover, FABC further modifies soil structure and solute transport dynamics (Qiu et al. 2021). And these findings suggest that pollutant transport in soil is governed by both adsorption and hydrodynamic processes. Nevertheless, the effects of biochar aging on soil solute transport remain inadequately understood. Previous research has disproportionately focused on adsorption effects while underestimating hydrodynamic influences, potentially skewing pollutant transport assessments (Zhou et al. 2016; Zou and Zheng 2013). Hence, equilibrium adsorption experiments alone provide insufficient insights into pollutant mobility.

Antibiotics have become a major group of emerging contaminants (ECs) worldwide (Danner et al. 2019; Lin et al. 2020). While strongly sorbing antibiotics like quinolones (QLs) and tetracyclines (TCs) have been extensively studied, more mobile compounds such as sulfonamides (SAs) and FF require further investigation due to their higher leaching potential (Biošić et al. 2017; Park and Huwe 2016). Notably, in Chinese urban

areas, antibiotics have been detected at concentrations above 0.01 μg kg^{-1}, with transport occurring via runoff and leaching from agricultural soils (Liu et al. 2022). SD and FF, commonly used in livestock farming, show high water solubility (77 and 1320 mg L^{-1}) and low log K_{ow} (−0.04 and −1.22) (Gao et al. 2015; He et al. 2019; Yin et al. 2019; Zou and Zheng 2013). Under typical experimental conditions (pH = 6.8 ± 0.3), although dissociable groups in the SD molecular structure (pK_a = 2.10, 6.48) theoretically induce localized polarization effects, macroscopic characterization confirms its overall apparent electroneutrality (Gao et al. 2015; He et al. 2019; Yin et al. 2019). As a consequence, for such weakly hydrophobic antibiotics, transport is dominated by instantaneous equilibrium adsorption (Zou and Zheng 2013). Recent studies have shown that biochar amendment increases soil K_f for SD and FF by 2.8 and 10.1 times, though this effect decreases after aging (Tang et al. 2024). Overall, biochar influences antibiotic transport through both adsorption enhancement and hydraulic property modification (Ivanova et al. 2023; Tang et al. 2024; Yi et al. 2020).

Current knowledge remains limited on FABC impacts on soil physicochemical properties and solute transport mechanisms. While previous studies have examined FBC or short-term aging effects of 3–6 months (Gámiz et al. 2019; Paetsch et al. 2018) to one year (He et al. 2019; Tang et al. 2024), long-term field aging effects are poorly understood. This study hypothesizes that aging modifies biochar surface properties, pore structure and soil particle interactions, subsequently affecting antibiotic transport behavior. Using SD and FF as model compounds, this study aimed to (1) characterize biochar's physicochemical evolution during field aging (0, 1 and 5 years); (2) evaluate the dynamic changes in antibiotic adsorption sites and capacity of aged biochar and its underlying mechanisms; (3) examine effects of aged biochar on dispersive effects and solute transport characteristics; and (4) simulate relationships between biochar aging, particle interactions and antibiotic transport using Hydrus 1D.

2 Material and methods

2.1 Experimental site, soil characteristics, and chemical reagents

The study was conducted in the central Sichuan Basin, southwest China (31°16′N, 105°27′E), where purple soil covers approximately 160,000 km^2 (He et al. 2019; Liu et al. 2024). The annual precipitation and mean temperature were 911.21 mm and 16.60 °C (2013–2019), respectively, with temperature in the region extremes from −8.50 ℃ to 38.30 °C. Purple soil is characterized by a shallow surface layer, high porosity, and poor aggregation, making it susceptible to water erosion and runoff pollutant transport during rainstorm events (Gbadegesin et al. 2022). The experimental plot (20 m × 5 m, 6° slope) consisted of calcareous purple soil containing 39.16% sand, 49.75% silt, and 11.10% clay, with a 15 cm cultivation layer and bulk density of 1.5 g cm^{-3}.

FBC (1 wt%) was applied to sloping farmland in May 2014, with 11.25 kg distributed across 100 m^2 subplots and mixed uniformly using a rotary tiller. Agricultural management followed a corn–wheat rotation system without additional agrochemical inputs. Fertilization consisted of urea (N ≥ 46.4%), superphosphate (P_2O_5 ≥ 12%), and potassium chloride (K_2O ≥ 60%). Samples collected in 2015 and 2019 represented one-year (ABC1) and five-year aged biochar (ABC5), respectively. FABC particles (ca. 2 mm) were carefully extracted in the field using tweezers and subsequently washed gently with deionized water in the laboratory until the wash solution became clear (He et al. 2019; Wang et al. 2020). This method was specifically designed to preserve the integrity of potential biochar–soil complexes within the pores. To avoid disrupting pore-retained substances, the study deliberately excluded aggressive ultrasonic or chemical treatments, focusing solely on removing surface-adhered soil particles. Since biochar pore structures undergo dynamic changes during soil aging, this method ensures a more accurate representation of pore-retained substances by maintaining their structural integrity throughout the aging process. After washing, the biochar particles were oven-dried at 60 °C for 24 h before characterization. Due to limitations in the experimental plot usage, the maximum long-term aging period investigated in this study was 5 years. Four treatments were established: control soil (S), fresh biochar-amended soil (SFBC), and aged biochar-amended soils (SABC1 and SABC5). Composite samples from five random sampling points per treatment were air-dried, sieved at 2 mm and stored for analysis, with their basic physicochemical properties shown in Table S1.

This investigation focused on weakly hydrophobic antibiotics, specifically SD and FF, with high purity (≥ 99.5%) from Dr. Ehrenstorfer GmbH (Table S2). Chromatographic-grade acetonitrile and methanol were supplied by Thermo Fisher Scientific, with reagents prepared using ultrapure water from a Millipore system (USA). Biochar was synthesized via slow pyrolysis at 500 °C under low oxygen conditions. This temperature represents an optimal balance between carbonization degree and pore development (Ivanova et al. 2023). The feedstocks used were a mixture of organic substances such as straws, stems, and haulms from agricultural residues by Sanli New Energy Co., Ltd. (Shangqiu, China).

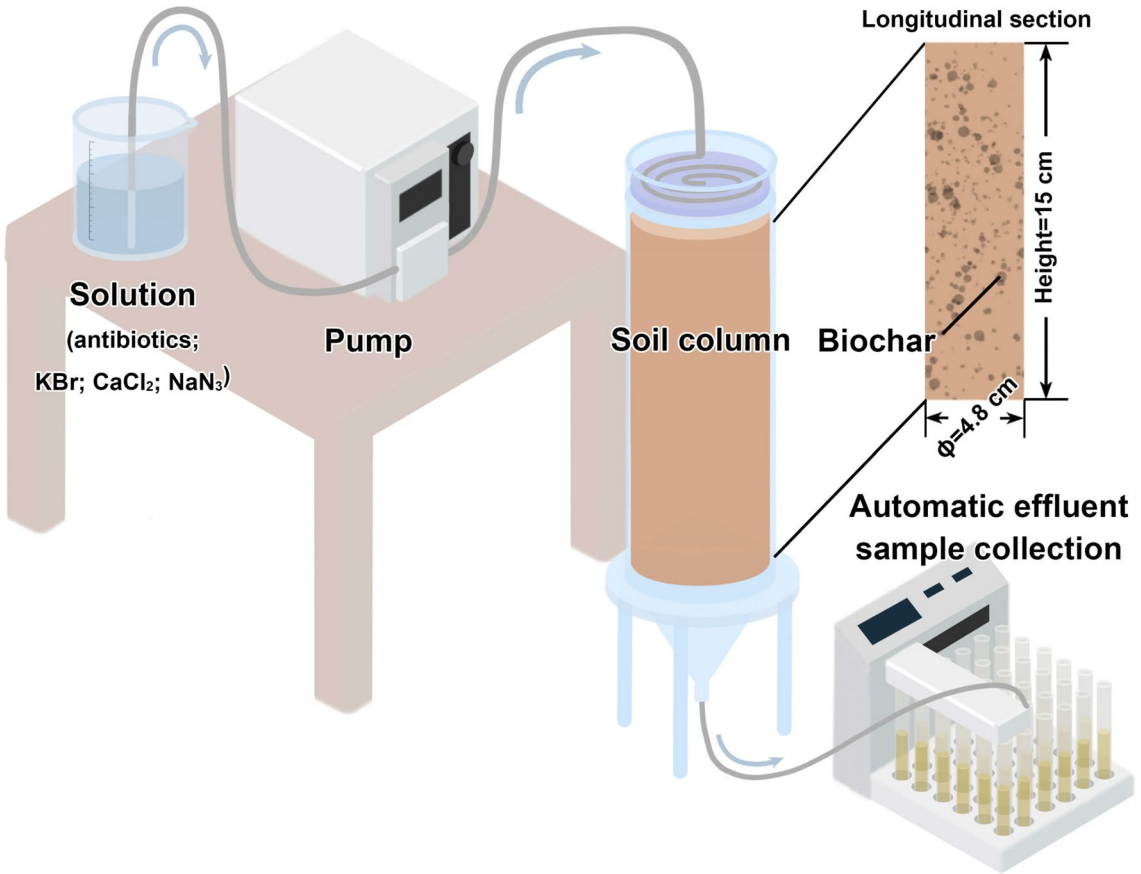

Fig. 1 Schematic diagram of the biochar-amended soil column experiment

2.2 Biochar characterization

Biochar characterization was performed using multiple analytical techniques. Elemental composition (C, H, O, N, TC, OC and TN) was quantified using an elemental analyzer (Elementar Vario El cube, Germany). Surface and structural properties were assessed via scanning electron microscopy–electron dispersion X-ray spectroscopy (SEM–EDS) (JSM-7500F, Japan Electronics Co., Ltd., Japan). N_2-adsorption isotherms were obtained at 77 K using an Autosorb-1 gas analyzer (ASAP 2460, Micromeritics, USA), with SSA determined by applying the Brunauer–Emmett–Teller equation. Biochar surface chemical composition was determined using Fourier transform infrared spectroscopy (FTIR) in the range of 400–4000 cm^{-1} with 2 cm^{-1} increments, and X-ray photoelectron spectroscopy (XPS) (NicoletIS50 and K-Alpha, Thermo Fisher Scientific Inc., USA). Cation exchange capacity (CEC) was measured using a nitrogen analyzer with an automatic distillation device (KDN-812, North–South Keyi Technology Co., Ltd., China).

2.3 Sorption–desorption and column experiments

Batch equilibration experiments for antibiotic sorption–desorption were conducted following OECD guideline 106 (OECD 2006). Each experiment involved 1 g of either untreated or biochar-amended soil with 10 mL of antibiotic solution (0–7.0 mg L^{-1}) in a glass tube. The experiment employed 0.01 mol L^{-1} $CaCl_2$ solution as ionic strength modifier and 0.1 g L^{-1} NaN_3 solution as microbial inhibitor (pH = 6.8 ± 0.3). $CaCl_2$ solution maintained natural soil solution characteristics while preserving CEC and solute transport dynamics. NaN_3 effectively suppressed microbial degradation processes. Photolytic reactions were minimized through aluminum foil light shielding. Samples were agitated for 24 h at 180 rpm, based on preliminary kinetics indicating sufficient equilibration. After agitation, the mixtures were centrifuged at 4000 rpm for 10 min. The supernatant was filtered through 0.22-μm membrane, followed by a 24-h desorption phase using 9 mL fresh $CaCl_2$ solution. All experiments were performed in triplicate at 25 °C.

Column experiments were conducted using 4.8 cm × 15 cm columns, with pore volumes (PV)

of 98.60–139.39 mL across treatments (Fig. 1) with characteristics detailed in Table S3. Bromide ion (Br^-) served as a tracer for evaluating water flow dynamics (Gbadegesin et al. 2022). Each column received 4 PV of solution (50 mg L^{-1} KBr, 1 mg L^{-1} antibiotics, 0.01 mol L^{-1} $CaCl_2$), followed by 2 PV of ultrapure water leaching. Flow rates simulated moderate rainfall (10–25 mm h^{-1}) using a peristaltic pump (BT-100F, Baoding Lange Co., Ltd.), ensuring soil columns saturation (Table S3). Br^- concentrations, electrical conductivity (EC), and colloid concentrations were measured using a Br^- detector (Bante931, Shanghai Bante Co., Ltd., China), conductivity meter (DDS-11A, Shanghai Leici Co., Ltd., China), and UV–Vis spectrophotometer (Bante931, Shanghai Bante Co., Ltd., China), respectively.

Antibiotic analysis was performed via Agilent 1290 Infinity II high-performance liquid chromatography with ultraviolet detection (HPLC–UV) system (USA) with a C18 column (150 mm × 2.1 mm, 3.5 mm, Waters, Milford, USA) at 30 °C. Mobile phase comprised 0.5% formic acid (A) and acetonitrile (B). The injection volume was 20 µL per sample, and the flow rate for gradient elution was 0.8 mL min^{-1}. The gradient elution program was as follows: 0–1 min: 80% A; 1–13.5 min: 80–70% A; 13.5–15 min: 70–80% A. Retention times for SD and FF were 3.9 and 7.3 min, with detection limits of 0.05 mg L^{-1}. Recovery rates were 84% for SD and 65% for FF. The antibiotic retention rate in soil column was quantified by comparing influent and effluent antibiotic fluxes through the soil column, expressed as a percentage of total retention.

2.4 Modeling

The K_d of the target antibiotics was determined using batch experiments and fitted with linear models (Eq. 1), indicating the partitioning behavior between soil and aqueous phases.

$$K_d = \frac{Q_e}{C_e} \tag{1}$$

where K_d is solid-water distribution coefficient (L kg^{-1}); Q_e is the amount adsorbed on the solid phase at equilibrium (mg g^{-1}); C_e is the solute concentration in the liquid phase at equilibrium (mg L^{-1}).

A one-dimensional water flow and solute transport simulation was conducted using the Hydrus 1D model to analyze the movement of Br^- tracer and antibiotics in soil (Gbadegesin et al. 2022). The convection–dispersion equation (CDE) (Eq. 2–4) was used to determine λ and D through Br^- data under equilibrium conditions, while the two-site chemical nonequilibrium model (TSM) (Eq. 5–7) was applied to obtain the mass transfer coefficient α and f from antibiotic breakthrough curves (BTCs) (Van Genuchten, 1989).

$$\frac{\partial c}{\partial t} = \frac{D}{R}\frac{\partial^2 c}{\partial x^2} - \frac{v}{R}\frac{\partial c}{\partial x} \tag{2}$$

$$R = 1 + \frac{\rho K_d}{\theta_v} \tag{3}$$

$$D \approx D_h = \lambda v \tag{4}$$

$$(1 + \frac{f\rho K_d}{\theta_v})\frac{\partial c}{\partial t} + \frac{\rho}{\theta_v}\frac{\partial S_2}{\theta_t} = D\frac{\partial^2 c}{\partial x^2} - v\frac{\partial c}{\partial x} \tag{5}$$

$$\frac{\partial S_1}{\theta_t} = fK_d\frac{\partial c}{\partial t} \tag{6}$$

$$\frac{\partial S_2}{\theta_t} = \alpha[(1-f)K_d c - S_2] \tag{7}$$

where c is solute concentration (mg L^{-1}); t is time (h); D is hydrodynamic dispersion coefficient (cm^2 h^{-1}); λ is dispersivity (cm); R is the dimensionless blocking factor; x is distance (cm); v is the average pore water velocity (cm h^{-1}); ρ is dry bulk weight (g cm^{-2}); θ_v is volumetric water content (cm^3 cm^{-3}); f is the fraction of transient adsorption exchange at equilibrium (dimensionless); S_1 and S_2 are the adsorption concentrations at the instantaneous and kinetic adsorption points (mg kg^{-1}), respectively; α is the first-order kinetic rate coefficient (h^{-1}).

Model accuracy was assessed using the coefficient of determination (R^2) and root mean square error (RMSE). R^2 values approaching 1 indicate high accuracy, while lower RMSE values reflect smaller error magnitudes.

2.5 Statistical analysis

Antibiotic sorption and desorption analyses utilized the Freundlich model for isotherm data and TSM for BTCs. Origin 2021 (Originlab, USA) was employed for batch equilibrium data fitting, figure creation, and coloring. XPS, FTIR and Raman spectra were normalized using min–max normalization in SPSS 22.0 (IBM Corp., Armonk, NY, USA). Statistical assessment of differences between FBC and ABC properties, and between control and biochar-amended soils, was conducted using one-way analysis of variance (ANOVA) in SPSS 22.0, with significance established at $p < 0.05$.

3 Results

3.1 Field aged biochar physicochemical evolution

SEM analysis (Fig. 2b) revealed morphological transformations from porous structure of FBC to smoothed surfaces of ABC1 and ABC5 with enlarged

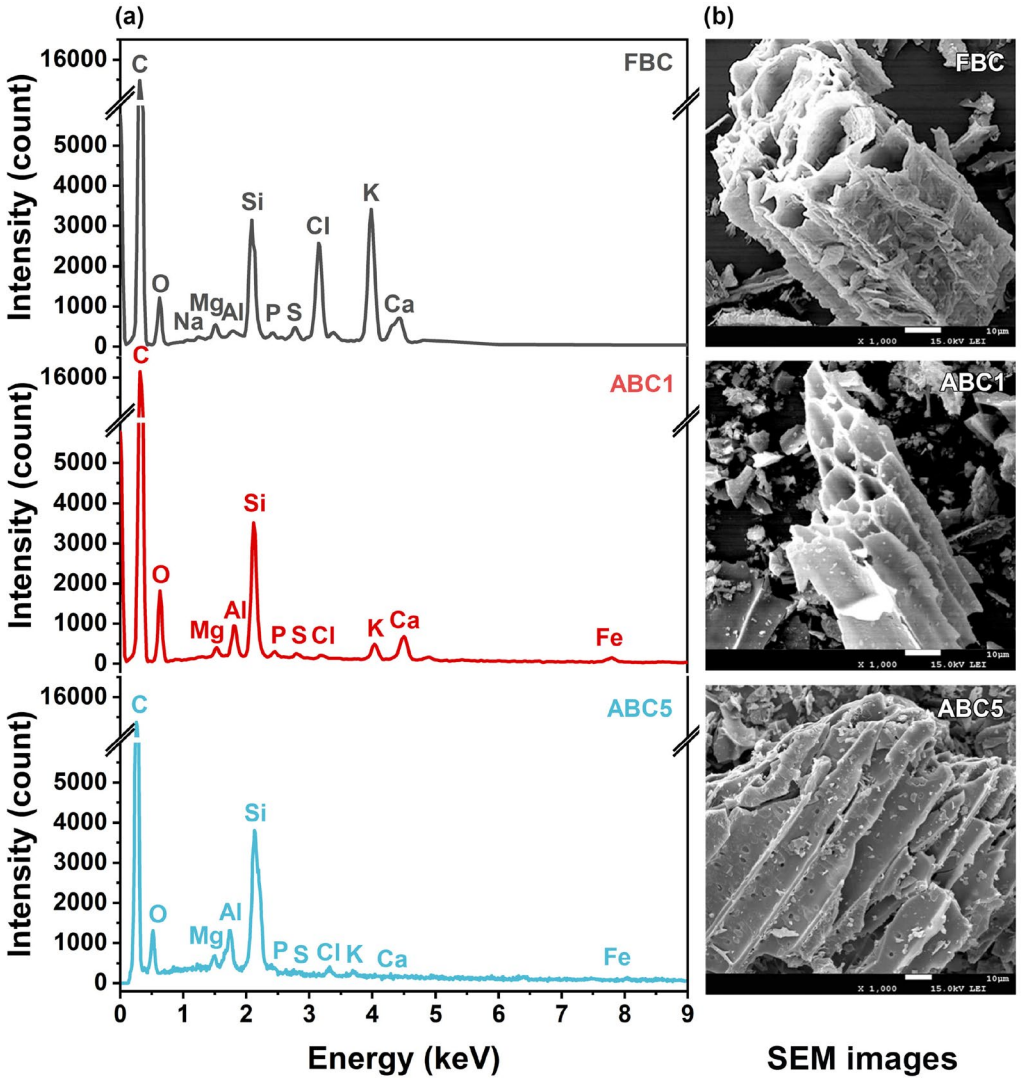

Fig. 2 Surface morphology and elements of FBC and ABC based on EDS (**a**) and SEM analysis (**b**)

pore diameters, corresponding to changes in SSA and pore characteristics. The SSA and average pore diameter demonstrated a non-linear response to aging, characterized by an initial increase followed by a subsequent decrease. The SSA increased from 6.95 $m^2\ g^{-1}$ in FBC to 13.85 $m^2\ g^{-1}$ in ABC1, before declining to 7.33 $m^2\ g^{-1}$ in ABC5. A similar pattern was observed for the average pore diameter, which increased from 7.13 mm in FBC to 13.57 mm in ABC1, and subsequently decreased to 7.72 mm in ABC5. Notably, aging induced non-linear morphological changes in surface properties of biochar, with initial enhancement followed by deterioration in SSA and pore characteristics.

EDS analysis revealed distinct temporal variations in the elemental composition of biochar surface (Fig. 2a). The soil minerals primarily comprised quartz (45.1%), plagioclase (14.5%), calcite (13.7%), montmorillonite (9.5%), and illite (10.5%), with minor contents of K-feldspar (2.6%) and hematite (0.6%). The mineral phases consisted of SiO_2-rich quartz, Al-rich silicates, and Fe-rich hematite. FBC exhibited characteristic C peak intensity (16,615 counts) with low O content (1,223 counts). During aging, C peaks decreased to 13,952 and 13,482 counts in ABC1 and ABC5, while O content showed nonlinear variation from 1,828 to 1,314 counts. Mineral elements (Fe, Al, and Si) emerged distinctively, with Si showing higher intensity in ABC1, while both Al and Si intensities increased in ABC5. The elemental composition and N_2 sorption characteristics of biochar at different aging stages are presented in Table 1, revealing

Table 1 The characteristics of biochar at different aging time

		FBC	ABC1	ABC5
Elemental composition	C (%)	80.18	75.91	71.84
	N (%)	1.53	1.73	2.50
	O (%)	16.04	20.50	22.54
	C/N	52.41	43.13	28.77
	O/C	0.20	0.27	0.31
	(N + O)/C	0.22	0.29	0.35
N_2-adsorption isotherms	BET surface area ($m^2\ g^{-1}$)	6.95	13.85	7.33
	Average pore diameter (mm)	7.13	13.57	7.72

substantial modifications in biochar properties over the five-year period. The C content decreased from 80.18% in FBC to 71.84% in ABC5, whereas N and O contents increased from 1.53% and 16.04% to 2.50% and 22.54%, respectively. These compositional changes were reflected in a 45.11% reduction in the C/N ratio (from 52.41 in FBC to 28.77 in ABC5) and a 55.00% increase in the O/C ratio (from 0.20 in FBC to 0.31 in ABC5). Correspondingly, the (N + O)/C ratio increased from 0.22 in FBC to 0.35 in ABC5. These results revealed progressive C content depletion with concurrent enrichment in O and N content, accompanied by increased mineral element intensities during aging.

XPS analysis of C1s spectra (Fig. 3, Figure S2) confirmed the surface oxidation during aging. FBC showed predominantly –C–C– and –C–H bonds (77%). ABC1 exhibited reduced aliphatic bonds (65%) with increased –C–O– groups (22%). ABC5 demonstrated further modifications with decreased –C–C– and –C–H bonds (48%) and increased –COOH groups (22%). Intermediate oxidized groups (–C = O and –C–O–) accounted for 19% and 11%, respectively. FTIR spectroscopy (Figure S1) revealed distinct modifications in biochar surface functional groups during the aging process. The spectra exhibited characteristic bands corresponding to hydroxyl (–O–H stretching at 3420 cm^{-1}), aliphatic (–C-H at 2920 and 2850 cm^{-1}), carboxylic (1560 and 1420 cm^{-1}), and polysaccharide groups. ABC1 displayed reduced hydroxyl peak intensity, while both ABC1 and ABC5 showed decreased aliphatic stretching vibrations. Enhanced carboxyl stretching and increased –C–O– vibrations (1100–900 cm^{-1}) in aged samples indicated progressive surface oxidation. These spectroscopic findings collectively demonstrate the progressive enhancement of surface polarity and hydrophilicity during biochar aging processes.

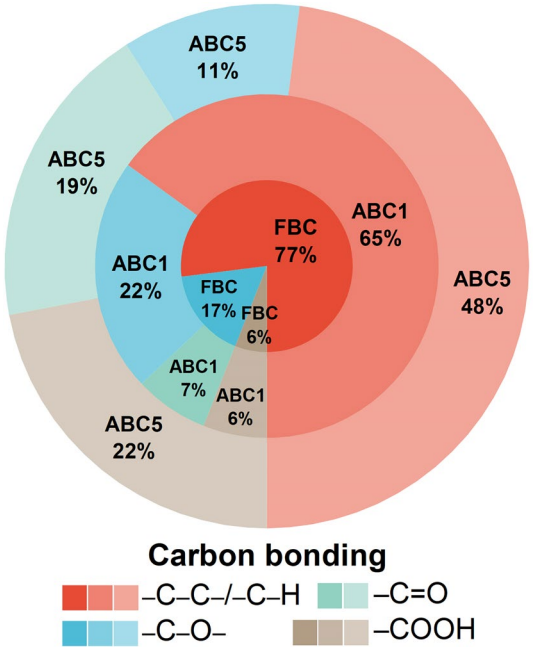

Fig. 3 Sunburst chart of XPS analysis of functional groups in FBC, ABC1, and ABC5

3.2 Antibiotic batch adsorption and breakthrough with aged biochar

Batch adsorption experiments (Fig. 4) demonstrated that SD and FF adsorption in biochar-amended soil followed linear isotherms (He et al. 2019; Liu et al. 2017b). The linear model effectively described the adsorption–desorption behavior with high correlation coefficients ($R^2 = 0.9772–0.9898$ for SD and 0.9766–0.9877 for FF, $p < 0.05$) (Table 2). The fitted slopes decreased in the order of SFBC > SABC1 > SABC5 > S (Fig. 4), indicating enhanced adsorption capacity by FBC amendment. SD showed lower affinity due to its polar sulfonamide group ($–SO_2NH_2$) (Gbadegesin et al. 2022; Peng et al. 2019), while FF exhibited stronger sorption attributed to its hydrophobic nature (He et al. 2019; Zou and Zheng 2013). Although biochar aging decreased its effectiveness, both SABC1 and SABC5 maintained higher adsorption capacities than S. The modification of biochar substantially enhances the pollutant adsorption capacity of soil. This enhancement significantly influences pollutant penetration and migration dynamics in soil systems. Notably, increased adsorption capacity results in elevated pollutant retention and reduced peak concentration, consequently decelerating the migration process. These observations can be substantiated through subsequent soil column experiments.

Soil column experiments are crucial for assessing pollutant safety and risk in soil environments (Pan and

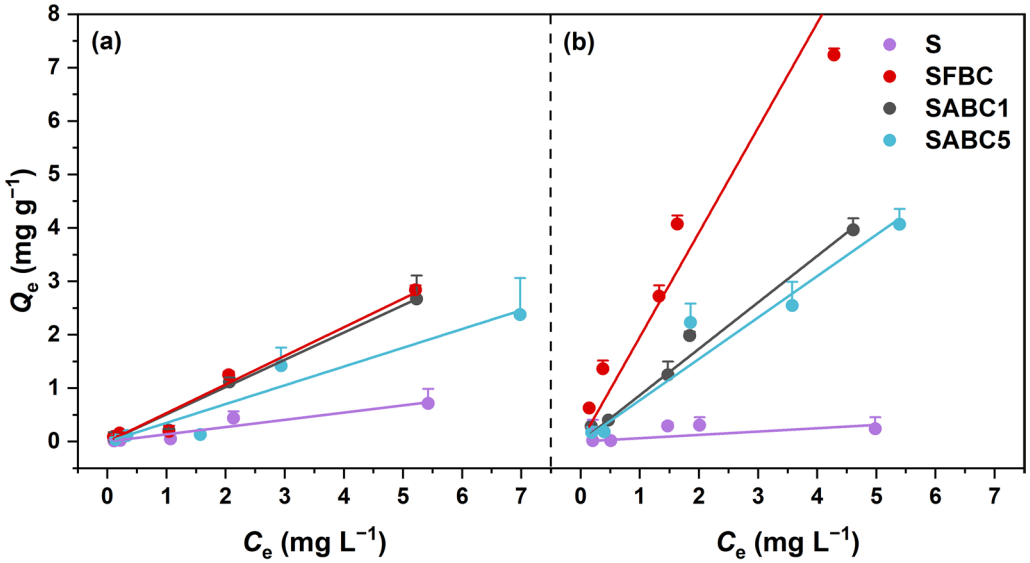

Fig. 4 Linear adsorption isotherms of SD (**a**), FF (**b**) on S, SFBC, SABC1 and SABC5

Table 2 Adsorption kinetics fitting parameters (K_d, λ, D, f, a) of CDE and TSM for SD and FF

		S	SFBC	SABC1	SABC5
Br^-	λ	0.4754 ± 0.0612	0.4364 ± 0.0531	0.8817 ± 0.0819	0.7817 ± 0.0852
	D	0.9745 ± 0.1255	0.7070 ± 0.0860	1.6047 ± 0.1491	1.2195 ± 0.1329
	R^2	0.9628	0.9858	0.9142	0.1531
	RMSE	0.0836	0.0542	0.1531	0.1065
SD	K_d	0.1355 ± 0.0142	0.5608 ± 0.0125	0.5354 ± 0.0476	0.3514 ± 0.0223
	f	0.0007 ± 0.0069	0.1000 ± 0.0227	0.3514 ± 0.0281	0.3021 ± 0.0255
	a	0.0141 ± 0.0039	0.0059 ± 0.0010	0.0192 ± 0.0056	0.0160 ± 0.0047
	R^2	0.9852	0.9898	0.9772	0.9791
	RMSE	0.0524	0.0407	0.0715	0.0611
FF	K_d	0.0623 ± 0.0224	1.9598 ± 0.1684	0.8692 ± 0.0237	0.7747 ± 0.0682
	f	0.0006 ± 0.0033	0.0544 ± 0.0030	0.3245 ± 0.0107	0.3129 ± 0.0131
	a	0.0179 ± 0.0022	0.0047 ± 0.0003	0.0183 ± 0.0028	0.0164 ± 0.0022
	R^2	0.9877	0.9834	0.9766	0.9816
	RMSE	0.0912	0.0429	0.0540	0.0503

K_d is solid-water distribution coefficient (L kg^{-1}); λ is the dispersivity (cm); D is hydrodynamic dispersion coefficient (cm^2 h^{-1}); f is the fraction of transient adsorption exchange at equilibrium (dimensionless); a is the first-order kinetic rate coefficient (h^{-1})

Chu 2017). The BTCs portray the relationship between relative solute concentration (C/C_0) in column effluent and PV, providing insights into the capacity of soil for organic pollutant retention (Lin et al. 2021) (Fig. 5). The BTC C/C_0 peak values follow the order FF < SD < Br^-, where Br^- served as a non-reactive tracer, indicating differential migration rates through the soil column. The addition of biochar delayed the emergence of antibiotic peaks by 0.2–0.3 PV compared to S. The BTCs exhibited characteristic asymmetry and tailing phenomena, suggesting that FABC enhanced both adsorption retention and desorption hysteresis.

Analysis of antibiotic retention rates revealed that SD achieved highest retention in SABC1 (16.57%), significantly exceeding the retention rates observed in S (5.03%) and SFBC (2.15%). The retention capacity remained at 12.55% in SABC5. Similarly, FF exhibited the highest retention in SABC1 (24.78%), followed closely by SABC5 (23.24%), exceeding those in S (19.74%) and SFBC (16.15%). Notably, the incorporation of both fresh and aged biochar resulted in substantial reductions in

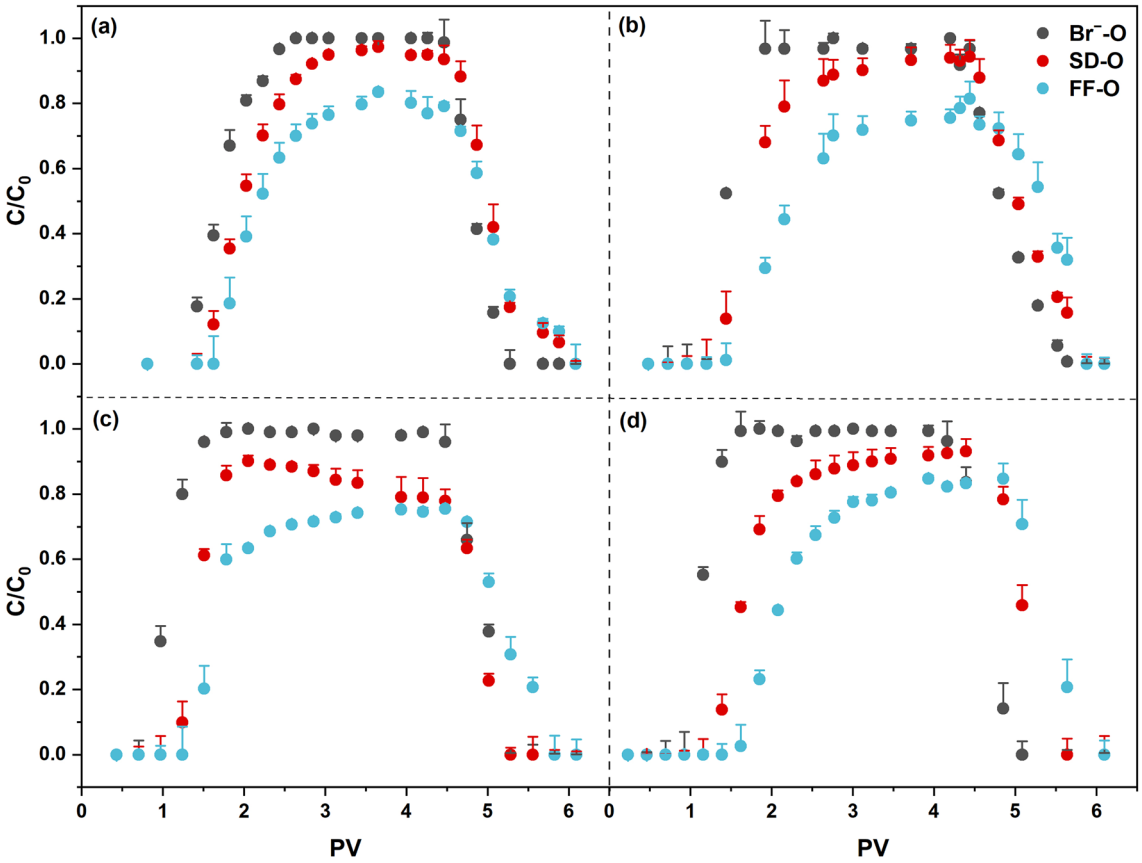

Fig. 5 Observed breakthrough points of tracer Br^-, SD and FF in (**a**) S, (**b**) SFBC, (**c**) SABC1 and (**d**) SABC5. C, the concentration of pollutants in the effluent; C_0, the concentration of pollutants in the influent; O, observed sample

peak concentrations by 92.55–96.83% for SD and 96.94–99.73% for FF.

3.3 Modeling

Linear model fitting (Table 2) revealed significant differences in K_d values across soil samples for both SD and FF treatments ($p < 0.05$). The obtained K_d values in S were 0.14 and 0.06 for SD and FF, respectively, with FF showing notably reduced adsorption capacity. Biochar incorporation significantly enhanced the K_d values in SFBC to 0.51 and 1.86 for SD and FF treatments ($p < 0.05$). A declining trend in K_d values was observed in aged biochar-amended soils, with SABC1 showing 0.54 (SD) and 0.87 (FF), while SABC5 exhibited 0.35 (SD) and 0.77 (FF). Despite the overall aging-induced decline, biochar demonstrated the strongest enhancement effect under FF conditions. Hydrus 1D model simulations demonstrated excellent agreement with BTCs, with R^2 values of 0.9672–0.9929 (Fig. 6). These results confirmed the capability of the model of effectively characterizing water flow and adsorption dynamics of Br^-, SD, and FF in soil. The C/C_0 of antibiotics followed a distinct sequence of SABC1 < SFBC < SABC5 < S. In S, peak C/C_0 values were recorded at 0.97 and 0.83 for SD and FF, respectively. The addition of FBC reduced these values to 0.94 and 0.81, while ABC1 further decreased them to 0.90 and 0.76. However, ABC5 showed slightly elevated peak concentrations.

The transport dynamics of Br^- in biochar-amended soils were evaluated using CDE model, focusing on λ and D values (Zhuang et al. 2021) (Table 2). In this context, λ values represent water and solute dispersion length scale, whereas D values quantify mechanical dispersion and molecular diffusion effects. Biochar aging enhanced hydrophilicity and surface roughness, increasing pollutant transport rates (Wang et al. 2019b). Compared to S (0.4754), SFBC showed decreased λ values (0.4364) ($p < 0.05$). In contrast, SABC1 and SABC5 demonstrated notably higher values of 0.8817 and 0.7817, respectively. Regarding dispersion coefficients, D values showed distinct variations across treatments, with SFBC showing low values (0.7070 $cm^2\ h^{-1}$) and SABC5 demonstrating

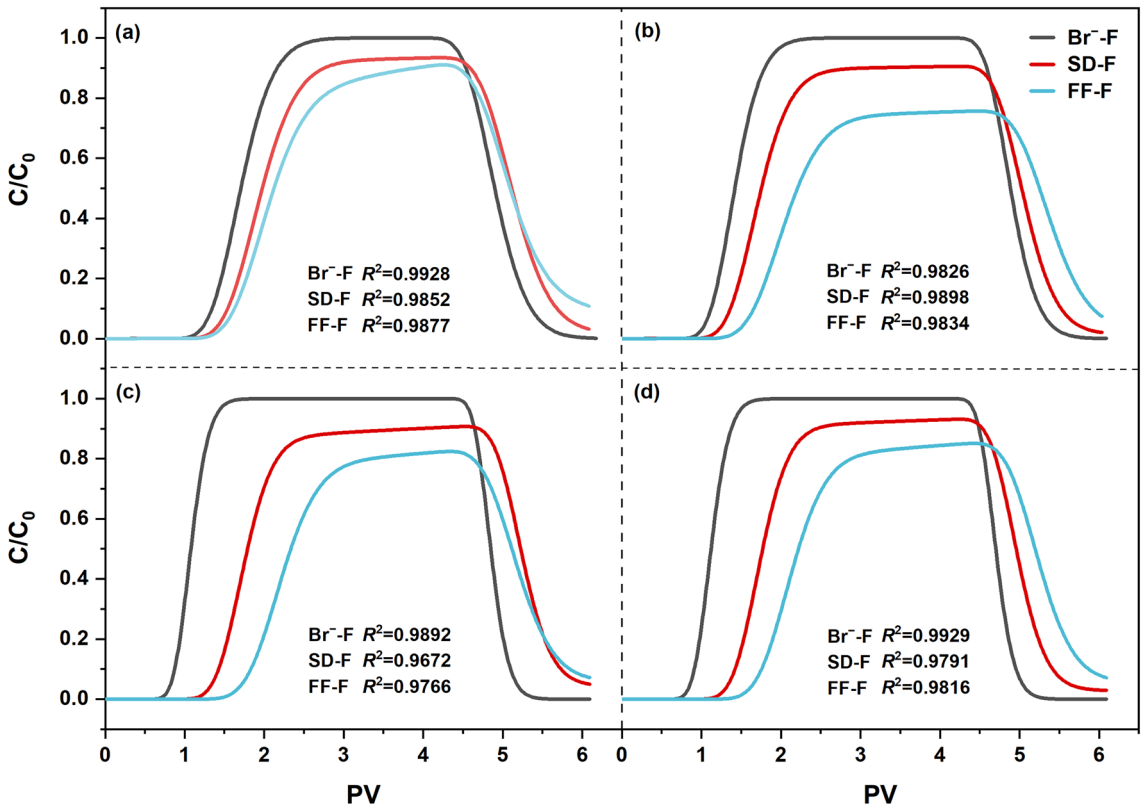

Fig. 6 Simulated breakthrough curves (BTCs) of tracer Br^-, SD and FF in (**a**) S, (**b**) SFBC, (**c**) SABC1 and (**d**) SABC5. F, fitted sample

the highest coefficient (1.2195 cm^2 h^{-1}), reflecting evolving soil hydrodynamic properties during aging.

Further insights are derived from analyzing the adsorption kinetics between biochar and antibiotics through TSM parameters f and α (Wei et al. 2019) (Table 2). The f value quantifies the proportion of adsorption sites at equilibrium with the solution phase, while α value represents the rate of solute transfer between equilibrium and kinetic adsorption sites. The f values revealed limited equilibrium adsorption capacity, predominantly below 0.1. However, SABC1 and SABC5 both maintained elevated f values between 0.30–0.36, representing 3.02–5.75 times increases compared to SFBC for both SD and FF. While SABC1 demonstrated higher proportions of equilibrium adsorption sites, SABC5 showed moderate decreases of 14.03% and 3.57% for SD and FF, respectively.

4 Discussion

4.1 Physicochemical properties alteration in biochar field aging

SEM results further validated these transformations, revealing an evolution from the highly porous and irregular structure of FBC to the smoothed, layered morphology with increased average pore diameter in ABC1 and ABC5. These alterations in surface properties and structural characteristics likely exert significant influence on adsorption capacity and water retention properties of biochar. It indicated that the aging process transforms biochar from a predominantly carbonaceous material into a composite matrix closely integrated with soil particles (Dong et al. 2017; Tan et al. 2019). The temporal evolution of biochar SSA and average pore diameter revealed distinct structural modifications throughout the aging process. The observed pattern, characterized by an initial increase followed by a subsequent decrease in SSA, resulted from nonlinear evolution of pore structure during aging. During early aging (ABC1), biochar particles underwent fragmentation and released dissolved organic matter (DOM), accompanied by the leaching of soluble organic compounds and ash, thereby generating more complex pore structures that resulted in enhanced SSA and pore diameters (Wang et al. 2020). Upon extended aging (ABC5), soil minerals (e.g., silicates, carbonates, and oxides) precipitated within biochar pores and formed complexes with organic matter, ultimately leading to pore occlusion and subsequent reductions in SSA and pore size (Wang et al. 2020). The results indicated that pore development was dominant in ABC1, whereas the

effects of mineral filling prevailed in ABC5. While Tan et al. (2019) documented initial decreases in biochar SSA during the first three years due to pore structure deterioration, the formation of new micropores in ABC5 contributed to a 23.91% increase in SSA compared to FBC. Supporting evidence demonstrated that ABC5 exhibited more than 100% increase in SSA, accompanied by a 17–106% enhancement in total PV (Dong et al. 2017). These structural modifications not only influenced the intrinsic properties of biochar but also potentially altered its interactions with soil particles through mechanisms such as competitive adsorption between DOM and soil particle surface sites, as well as micropore occlusion, thereby affecting its environmental behavior.

Elemental composition and EDS analysis revealed distinct oxidation and mineralization processes during biochar aging. The observed reduction in C content accompanied by increases in N and O contents from FBC to ABC5, coupled with decreased C/N ratio and elevated O/C ratio, indicated the dissolution of labile C components and formation of oxygen-containing functional groups (Mia et al. 2017; Quan et al. 2020; Tan et al. 2020, 2019). These modifications likely enhanced polarity and surface reactivity of biochar, subsequently influencing its environmental behavior. Dong et al. (2017) reported that aged biochar contained 2.44% less C and 30.88% more O compared to FBC. The oxidation process typically facilitates C loss through mineralization (Wang et al. 2020), explaining the observed decrease in C content. These changes reflected the progressive oxidation and decomposition of organic components of biochar (Kong et al. 2014). The evolution of Fe, Al, and Si elements suggest the development of interactions between biochar and soil particles (Lin et al. 2012; Yang et al. 2016). ABC1 showed a significant increase in Si content with minimal Al/Fe elevation, corresponding to predominant physical adsorption of silicate minerals (Yang et al. 2016). For ABC5, elevated Al and Si peak intensities suggest additional Al–O–C covalent bonds formation with clay minerals (e.g., kaolinite or montmorillonite), beyond physical adsorption (Jing et al. 2022). The enhancement in Fe content, particularly pronounced in ABC5, likely originated from soil-derived iron oxides. These modifications reflect the progressive coverage of biochar surfaces by soil particles, facilitating stronger biochar–soil interactions (Yang et al. 2016). Analysis of the soil mineral composition reveals that during the aging process, driven by a wet–dry cycles, mineral particles deposit within the pores through mechanical action (Dong et al. 2017).

FTIR and XPS analysis revealed significant changes in biochar functional groups during aging. Variations in the hydroxyl region were attributed to alcohols, phenols, and acids, with attenuated –OH peaks in ABC1 indicating reduced surface –OH content (Mia et al. 2017). Changes in the aliphatic region suggested decreased hydrocarbon content (Bekiaris et al. 2016; Suman et al. 2021), while enhanced carboxyl vibrations demonstrated increased carboxylic acids presence (Dong et al. 2017). The intensification of –C–O– stretching peaks indicated polysaccharide formation (Bekiaris et al. 2016). The characteristic band red shift suggested methyl group substitution by electron-donating groups (Balan et al. 2019).

While FABC (ABC1/ABC5) demonstrated superior SSA, pore diameter, and O/C ratio relative to FBC (Table 1), FBC exhibited enhanced adsorption capacity for weakly hydrophobic antibiotics due to mechanistic shifts. XPS analysis revealed the surface of FBC comprised 77% hydrophobic aromatic moieties (–C–C/–C–H), facilitating adsorption primarily through hydrophobic partitioning (Wei et al. 2019). Although oxidative aging increases SSA of FABC, introduced oxygen functionalities (–C–O–/–OH) elevate hydrophilicity, diminishing hydrophobic interactions. This transforms the dominant adsorption mechanisms to hydrogen bonding and π-π electron donor–acceptor (EDA) interactions (Peng et al. 2019). For weakly hydrophobic antibiotics, where hydrophobic partitioning remains the critical adsorption driver, structural configuration of FBC provides superior retention capacity. Notably, despite altered the dominant adsorption mechanisms in aged biochar, the biochar still maintains a certain adsorption stability over the long term.

4.2 Hydrodynamic dispersion and its effect with biochar

Hydrodynamic dispersion is an important factor in solute transport in soil. Hydrus 1D model inversion revealed distinct variations in D and α during biochar aging. D values showed an initial decrease followed by a gradual increase over the aging period (Fig. 7a). The SFBC treatment exhibited significantly lower D values compared to S, while D values increased progressively in SABC1 and SABC5. These changes indicated the evolution of soil pore structure and hydrodynamic properties during aging. The initial decrease in D values was attributed to SFBC hydrophobicity that limited water–soil contact and impeded water movement (Lei et al. 2020; Sun et al. 2015).

During the aging process, biochar formed complex pore networks and micro-aggregates with soil particles, leading to increased soil heterogeneity. The enhanced hydrophilicity of biochar surfaces and intricate pore structures improved water conductivity, thereby facilitating antibiotic transport as evidenced by

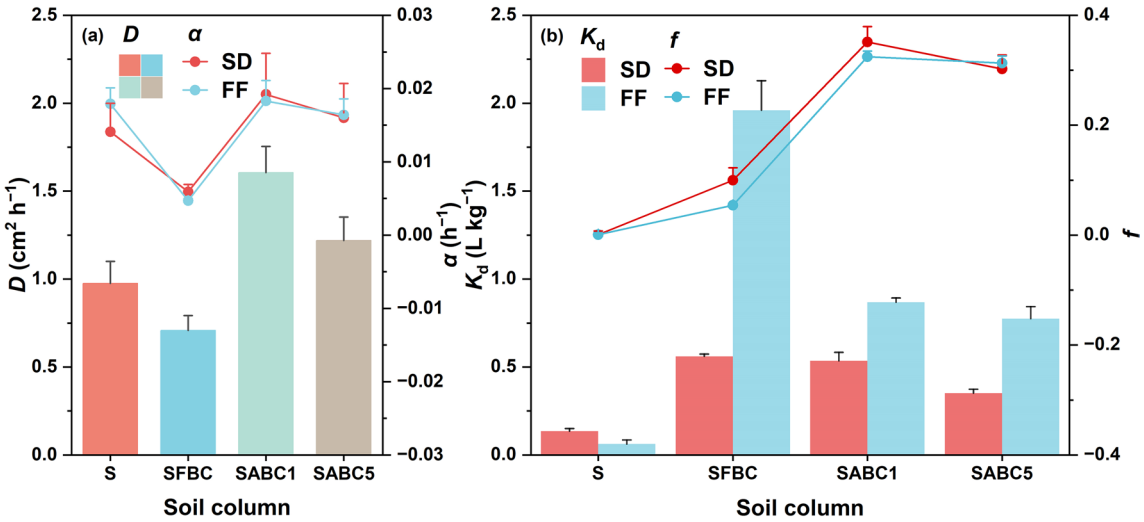

Fig. 7 Fitting parameters (**a**) *D*, *α* and (**b**) K_d, *f* of adsorption kinetics changes in biochar aging. *D*, hydrodynamic dispersion coefficient ($cm^2\ h^{-1}$); α, the first-order kinetic rate coefficient (h^{-1}); K_d, solid-water distribution coefficient ($L\ kg^{-1}$); *f*, the fraction of transient adsorption exchange at equilibrium (dimensionless)

increased *D* values (Cao et al. 2017; Dong et al. 2017; Nan et al. 2021). Biochar coating on soil particles created hydrophilic porous membranes with high polar surface energy, enhancing water retention capacity (Duan et al. 2021; Liu et al. 2017a; Wang et al. 2019a). Studies revealed that SABC treatment increased soil water content by 1.4% compared to S (Ivanova et al. 2023). These changes in water distribution directly reflected in *D* value variations, subsequently affecting antibiotic transport.

Analysis of *α* values further supported these findings. SFBC showed significantly lower *α* values ($p < 0.05$), suggesting unrealized regulatory potential of biochar and a non-equilibrium state. With aging progression, the increasing *α* values indicated the gradual approach toward equilibrium of the soil system. SABC1 displayed higher equilibrium ratios than SABC5, attributed to abundant DOC in FBC that enhanced binding of weakly hydrophobic antibiotics to soil particles (Wei et al. 2019). These modifications improved soil physical properties and water transport capacity while facilitating vertical antibiotic movement (Wang et al. 2019b). The impact of biochar aging on soil structure and antibiotic adsorption thus requires investigation across multiple temporal stages.

The impacts of biochar aging on soil structure and soil-biochar interactions can be characterized in three distinct stages. Initially, FBC exhibits hydrophobicity that directs water and solute toward soil particles (He et al. 2019). This limits antibiotic interactions with biochar, resulting in insignificant effects of biochar application (Jeffery et al. 2015). During the medium-term stage (one year), biochar surfaces transform from hydrophobic to hydrophilic, accompanied by increased oxygen-containing functional groups that enhance soil particle interactions (Mao et al. 2019; Usevičiūtė et al. 2021). These modifications alter soil porosity and water distribution, with 9–19% of biochar contributing to vertical transport and 20–53% facilitating lateral movement through surface runoff (Major et al. 2010; Obia et al. 2017). In the long-term stage (five years), aged biochar increases soil porosity and dispersivity, promoting antibiotic transport, although these effects may diminish due to structural degradation or mineral interactions (Dong et al. 2017).

4.3 Effect on biochar adsorption sites and antibiotic adsorption capacity

As shown in Fig. 7(b), biochar amendment exhibited significant effects on soil K_d and *f* values. The SFBC showed higher K_d values for both SD and FF compared to S. Liu et al. (2017b) found that biochar addition increased the K_d value of SD from 5.04 L kg^{-1} to 6.08 L kg^{-1}. As aging time increased, K_d values for SABC1 and SABC5 gradually decreased but remained higher than S, indicating the persistent effect of biochar amendment. Yin et al. (2019) also reported that K_d values for SD and FF in S were 0.04 L kg^{-1} and 0.10 L kg^{-1}, respectively, while in SABC1, K_d value of SD increased from 0.39 L kg^{-1} to 0.50 L kg^{-1}, and K_d value of FF decreased from 1.79 L kg^{-1} to 0.86 L kg^{-1}. SFBC demonstrated the strongest antibiotic sorption capacity, primarily attributed to its unique physicochemical properties including hydrophobic surfaces, high SSA and diverse functional groups. During aging, surface oxidation

increased oxygen-containing groups and hydrophilicity, while DOM release and mineral deposition altered pore structures, leading to decreased K_d values. Nevertheless, SABC5 maintained significantly higher sorption capacity than S ($p < 0.05$).

Changes in f values revealed the transformation of sorption site characteristics during biochar aging. The aging process optimized the sorption equilibrium distribution of antibiotics in soil, reflected in the overall increasing trend of f values for both SD and FF, suggesting that biochar aging could increase sorption sites (Khorram et al. 2017). SABC1 showed optimal sorption capacity due to moderate surface oxidation, which maintained sufficient sorption sites while forming oxygen-containing functional groups (Li et al. 2022). The formation of stable biochar–soil complexes and optimized pore structures contributed to enhanced antibiotic retention (Wei et al. 2019). The decreased f values in SABC5 suggested structural deterioration from prolonged aging and excessive oxidation, indicating biochar aging as a dynamic equilibrium process with stage-specific mechanisms.

The temporal variations in K_d and f values revealed that biochar gradually developed into stable composite systems with soil through aging processes. Although the pure antibiotic sorption capacity decreased over time, the overall remediation effectiveness was maintained to a certain extent. Notably, one-year aging emerged as a critical point when physicochemical properties of biochar reached optimal conditions, exhibiting strong sorption capacity while forming stable sorption structures. The soil improvement effects of biochar remained detectable even after 5-year aging.

5 Conclusion and outlook

A systematic investigation was conducted to examine biochar aging processes in purple soil over one-year and five-year periods, focusing on physicochemical properties evolution, adsorption behavior and hydrological characteristics. Results revealed that aging led to significant C loss in biochar structure, accompanied by increased O content and surface oxygen-containing functional groups. The SSA exhibited an initial increase followed by a decrease, reflecting dynamic alterations in elemental composition and pore structure. While antibiotics in SFBC showed high K_d values, its hydrophobicity limited antibiotic interactions. SABC1 demonstrated enhanced f and α values due to surface transition from hydrophobic to hydrophilic. Despite decreased K_d values, SABC5 formed stable composites with soil particles, maintaining effective remediation through improved λ and D values. These findings indicate that antibiotic transport shifts from adsorption-dominated to dispersion-influenced mechanisms, with biochar achieving long-term regulation via optimized soil structure and water movement.

As a promising soil amendment, the long-term effectiveness of biochar is crucial for environmental remediation assessment. Research on biochar application and aging stability contributes to soil quality improvement. Future research should extend to long-term effects under different soil types and climatic conditions, as well as mechanisms targeting specific environmental organic pollutants, to promote precise application of biochar technology in environmental management.

Supplementary Information

The online version contains supplementary material available at https://doi.org/10.1007/s42773-025-00460-4.

Additional file 1

Acknowledgements
We would like to thank Dr. Weizhen Fang at the Analysis and Testing Center of Southwest Jiaotong University for his assistance with antibiotic concentration analysis.

Author contributions
All authors contributed to the study conception and design. Xinyu Liu, Yang He, Jinghan Li, and Jiahui Li performed material preparation, data collection, and analysis. Xinyu Liu drafted the initial manuscript, with Yang He providing supervision and methodology input. Jinghan Li and Jiahui Li were responsible for software implementation and data curation. Jianqiang Zhang supervised the project and funding. Xiangyu Tang provided conceptualization, resources, and funding acquisition. All authors read and approved the final manuscript.

Funding
This work was supported by Natural Science Foundation of Sichuan Province, China (2024NSFSC0837), the Fundamental Research Funds for the Central Public-interest Scientific Institution (2024YYSKY-05), the Open Research Fund of Key Laboratory of Eco-industry of Ministry of Ecology and Environment, Chinese Research Academy of Environmental Sciences (2024KFF-04) and the Key Research and Development Program of Ganzi Prefecture's Science and Technology Plan (24kjjh0005).

Availability of data and materials
The datasets used or analyzed during the current study are available from the corresponding author upon reasonable request.

Declarations

Competing interests
All authors certify that they have no affiliations with or involvement in any organization or entity with any financial interest or non-financial interest in the subject matter or materials discussed in this manuscript.

Author details
[1]School of Environmental Science and Engineering, Southwest Jiaotong University, Chengdu 611756, China. [2]Institute of Mountain Hazards and Environment, Chinese Academy of Sciences, Chengdu 610299, China. [3]Sichuan Engineering Research Center for Pollution Control in Rail Transit Engineering, Chengdu 611756, China. [4]Sichuan International Science and Technology Cooperation Base for Intelligent Environmental Protection and Sustainable Development in Rail Transit, Chengdu 611756, China.

[5]State Key Laboratory of Subtropical Silviculture, Zhejiang A&F University, Hangzhou 311300, China.

Received: 20 November 2024 Revised: 1 March 2025 Accepted: 8 March 2025
Published online: 15 April 2025

References

Balan V, Mihai CT, Cojocaru FD, Uritu CM, Dodi G, Botezat D, Gardikiotis I (2019) Vibrational spectroscopy fingerprinting in medicine: from molecular to clinical practice. Materials. https://doi.org/10.3390/ma12182884

Bekiaris G, Peltre C, Jensen LS, Bruun S (2016) Using FTIR-photoacoustic spectroscopy for phosphorus speciation analysis of biochars. Spectrochim Acta A 168:29–36. https://doi.org/10.1016/j.saa.2016.05.049

Biošić M, Mitrevski M, Babić S (2017) Environmental behavior of sulfadiazine, sulfamethazine, and their metabolites. Environ Sci Pollut R 24(10):9802–9812. https://doi.org/10.1007/s11356-017-8639-8

Cao T, Chen W, Yang T, He T, Liu Z, Meng J (2017) Surface characterization of aged biochar incubated in different types of soil. BioResources 12:6366–6377. https://doi.org/10.15376/biores.12.3.6366-6377

Danner MC, Robertson A, Behrends V, Reiss J (2019) Antibiotic pollution in surface fresh waters: occurrence and effects. Sci Total Environ 664:793–804. https://doi.org/10.1016/j.scitotenv.2019.01.406

Dong X, Li G, Lin Q, Zhao X (2017) Quantity and quality changes of biochar aged for 5 years in soil under field conditions. CATENA 159:136–143. https://doi.org/10.1016/j.catena.2017.08.008

Duan M, Liu G, Zhou B, Chen X, Wang Q, Zhu H, Li Z (2021) Effects of modified biochar on water and salt distribution and water-stable macro-aggregates in saline-alkaline soil. J Soils Sediments 21(6):2192–2202. https://doi.org/10.1007/s11368-021-02913-2

Gámiz B, Velarde P, Spokas KA, Celis R, Cox L (2019) Changes in sorption and bioavailability of herbicides in soil amended with fresh and aged biochar. Geoderma 337:341–349. https://doi.org/10.1016/j.geoderma.2018.09.033

Gao L, Shi Y, Li W, Liu J, Cai Y (2015) Occurrence and distribution of antibiotics in urban soil in Beijing and Shanghai China. Environ Sci Pollut Res 22(15):11360–11371. https://doi.org/10.1007/s11356-015-4230-3

Gbadegesin LA, Liu XY, Tang XY, Liu C, Cui JF (2022) Leaching of sulfadiazine and florfenicol in an Entisol of a chicken-raising orchard: Impact of manure-derived dissolved organic matter. Agronomy 12(12):3228. https://doi.org/10.3390/agronomy12123228

He Y, Liu C, Tang XY, Xian QS, Zhang JQ, Guan Z (2019) Biochar impacts on sorption-desorption of oxytetracycline and florfenicol in an alkaline farmland soil as affected by field ageing. Sci Total Environ 671:928–936. https://doi.org/10.1016/j.scitotenv.2019.03.414

Ivanova N, Obaeed GLO, Sulkarnaev F, Buchkina N, Gubin A, Yurtaev A (2023) Effect of biochar aging in agricultural soil on its wetting properties and surface structure. Biochar 5(1):75. https://doi.org/10.1007/s42773-023-00272-4

Jeffery S, Meinders MBJ, Stoof CR, Bezemer TM, Van de Voorde TFJ, Mommer L, Van Groenigen JW (2015) Biochar application does not improve the soil hydrological function of a sandy soil. Geoderma 251–252:47–54. https://doi.org/10.1016/j.geoderma.2015.03.022

Jing F, Sun Y, Liu Y, Wan Z, Chen J, Tsang DCW (2022) Interactions between biochar and clay minerals in changing biochar carbon stability. Sci Total Environ 809:151124. https://doi.org/10.1016/j.scitotenv.2021.151124

Khorram MS, Lin D, Zhang Q, Zheng Y, Fang H, Yu Y (2017) Effects of aging process on adsorption-desorption and bioavailability of fomesafen in an agricultural soil amended with rice hull biochar. J Environ Sci 56:180–191. https://doi.org/10.1016/j.jes.2016.09.012

Kong LL, Liu WT, Zhou QX (2014) Biochar: an effective amendment for remediating contaminated soil. Rev Environ Contam Toxicol 228:83–99. https://doi.org/10.1007/978-3-319-01619-1_4

Lei W, Tang X, Zhou X (2020) Biochar amendment effectively reduces the transport of 3,5,6-trichloro-2-pyridinol (a main degradation product of chlorpyrifos) in purple soil: experimental and modeling. Chemosphere 245:125651. https://doi.org/10.1016/j.chemosphere.2019.125651

Li Y, He J, Qi H, Li H, Boyd SA, Zhang W (2020) Impact of biochar amendment on the uptake, fate and bioavailability of pharmaceuticals in soil-radish systems. J Hazard Mater 398:122852. https://doi.org/10.1016/j.jhazmat.2020.122852

Li J, Ouyang F, Zheng S, Liu X, He Y, Ren S (2022) Effects of biochar on sorption and transport of florfenicol in purple soil. Res Environ Sci 35(6):1467–1474. https://doi.org/10.1319/j.issn.1001-6929.2022.03.20

Lin Y, Munroe P, Joseph S, Kimber S, Van Zwieten L (2012) Nanoscale organo-mineral reactions of biochars in ferrosol: an investigation using microscopy. Plant Soil 357(1):369–380. https://doi.org/10.1007/s11104-012-1169-8

Lin X, Xu J, Keller AA, He L, Gu Y, Zheng W, Sun D, Lu Z, Huang J, Huang X, Li G (2020) Occurrence and risk assessment of emerging contaminants in a water reclamation and ecological reuse project. Sci Total Environ 744:140977. https://doi.org/10.1016/j.scitotenv.2020.140977

Lin Q, Li B, Liu X, Zhang B, Xu S (2021) Insights into sorption and leaching behavior of sulfadiazine in soil as affected by humic acid. J Soils Sediments 22(3):809–817. https://doi.org/10.1007/s11368-021-03110-x

Liu Z, Dugan B, Masiello CA, Gonnermann HM (2017a) Biochar particle size, shape, and porosity act together to influence soil water properties. PLoS ONE 12(6):e0179079. https://doi.org/10.1371/journal.pone.0179079

Liu Z, Han Y, Jing M, Chen J (2017b) Sorption and transport of sulfonamides in soils amended with wheat straw-derived biochar: Effects of water pH, coexistence copper ion, and dissolved organic matter. J Soils Sediments 17(3):771–779. https://doi.org/10.1007/s11368-015-1319-8

Liu XY, Zhang JQ, Gbadegesin LA, He Y (2022) Modelling approaches for linking the residual concentrations of antibiotics in soil with antibiotic properties and land-use types in the largest urban agglomerations in China: a review. Sci Total Environ 838:156141. https://doi.org/10.1016/j.scitotenv.2022.156141

Liu XY, Gu XY, Liu C, Gbadegesin LA, He Y, Zhang JQ (2024) Field migration of veterinary antibiotics via surface runoff from chicken-raising orchard in responding to natural rainfalls. Sci Total Environ 909:168527. https://doi.org/10.1016/j.scitotenv.2023.168527

Major J, Lehmann J, Rondon M, Goodale C (2010) Fate of soil-applied black carbon: Downward migration, leaching and soil respiration. Glob Change Biol 16(4):1366–1379. https://doi.org/10.1111/j.1365-2486.2009.02044.x

Mao J, Zhang K, Chen B (2019) Linking hydrophobicity of biochar to the water repellency and water holding capacity of biochar-amended soil. Environ Pollut 253:779–789. https://doi.org/10.1016/j.envpol.2019.07.051

Martin SM, Kookana RS, Van Zwieten L, Krull E (2012) Marked changes in herbicide sorption-desorption upon ageing of biochars in soil. J Hazard Mater 231–232:70–78. https://doi.org/10.1016/j.jhazmat.2012.06.040

Mia S, Dijkstra FA, Singh B (2017) Aging induced changes in biochar's functionality and adsorption behavior for phosphate and ammonium. Environ Sci Technol 51(15):8359–8367. https://doi.org/10.1021/acs.est.7b00647

Nan Q, Hu S, Qin Y, Wu W (2021) Methane oxidation activity inhibition via high amount aged biochar application in paddy soil. Sci Total Environ 796:149050. https://doi.org/10.1016/j.scitotenv.2021.149050

Obia A, Børresen T, Martinsen V, Cornelissen G, Mulder J (2017) Vertical and lateral transport of biochar in light-textured tropical soils. Soil till Res 165:34–40. https://doi.org/10.1016/j.still.2016.07.016

OECD (2006) Test no. 106: adsorption-desorption using a batch equilibrium method. OECD Guidel Test Chem 1:1–44

Omondi MO, Xia X, Nahayo A, Liu X, Korai PK, Pan G (2016) Quantification of biochar effects on soil hydrological properties using meta-analysis of literature data. Geoderma 274:28–34. https://doi.org/10.1016/j.geoderma.2016.03.029

Paetsch L, Mueller CW, Kögel-Knabner I, Von Lützow M, Girardin C, Rumpel C (2018) Effect of in-situ aged and fresh biochar on soil hydraulic conditions and microbial C use under drought conditions. Sci Rep 8(1):6852. https://doi.org/10.1038/s41598-018-25039-x

Pan M, Chu LM (2017) Leaching behavior of veterinary antibiotics in animal manure-applied soils. Sci Total Environ 579:466–473. https://doi.org/10.1016/j.scitotenv.2016.11.072

Park JY, Huwe B (2016) Effect of pH and soil structure on transport of sulfonamide antibiotics in agricultural soils. Environ Pollut 213:561–570. https://doi.org/10.1016/j.envpol.2016.01.089

Peng J, Wu E, Wang N, Quan X, Sun M, Hu Q (2019) Removal of sulfonamide antibiotics from water by adsorption and persulfate oxidation process. J Mol Liq 274:632–638. https://doi.org/10.1016/j.molliq.2018.11.034

Qiu L, Wu J, Qian Y, Nafees M, Zhang J, Du W, Yin Y, Guo H (2021) Impact of biochar-induced vertical mobilization of dissolved organic matter, sulfamethazine and antibiotic resistance genes variation in a soil-plant system. J Hazard Mater 417:126022. https://doi.org/10.1016/j.jhazmat.2021.126022

Quan G, Fan Q, Zimmerman AR, Sun J, Cui L, Wang H, Gao B, Yan J (2020) Effects of laboratory biotic aging on the characteristics of biochar and its water-soluble organic products. J Hazard Mater 382:121071. https://doi.org/10.1016/j.jhazmat.2019.121071

Ren X, Sun H, Wang F, Zhang P, Zhu H (2018) Effect of aging in field soil on biochar's properties and its sorption capacity. Environ Pollut 242(Pt B):1880–1886. https://doi.org/10.1016/j.envpol.2018.07.078

Suman S, Yadav AM, Jain T, Sk AA (2021) Study in the changes on the functional groups present in biomass during pyrolysis process. IOP Conf Ser: Mater Sci Eng. https://doi.org/10.1088/1757-899x/1146/1/012023

Sun H, Brewer CE, Masiello CA, Zygourakis K (2015) Nutrient transport in soils amended with biochar: a transient model with two stationary phases and intraparticle diffusion. Ind Eng Chem Res 54:4123–4135. https://doi.org/10.1021/ie503893t

Tan L, Sun C, Wang Y, Wang T, Wu GL, He H, Zheng J (2019) Changes in biochar properties in typical loess soil under a 5-year field experiment. J Soils Sediments 20(1):340–351. https://doi.org/10.1007/s11368-019-02398-0

Tan L, Ma Z, Yang K, Cui Q, Wang K, Wang T, Wu GL, Zheng J (2020) Effect of three artificial aging techniques on physicochemical properties and Pb adsorption capacities of different biochars. Sci Total Environ 699:134223. https://doi.org/10.1016/j.scitotenv.2019.134223

Tang XY, Yin WM, Yang G, Cui JF, Cheng JH, Yang F, Li XY, Wu CY, Zhu SG (2024) Biochar reduces antibiotic transport by altering soil hydrology and enhancing antibiotic sorption. J Hazard Mater 472:134468. https://doi.org/10.1016/j.jhazmat.2024.134468

Usevičiūtė L, Baltrėnaitė-Gedienė E, Baltrėnas P (2021) Hydrophilicity enhancement of low-temperature lignocellulosic biochar modified by physical-chemical techniques. J Mater Cycles Waste 23(5):1838–1854. https://doi.org/10.1007/s10163-021-01255-y

Van Genuchten MT, Wagenet RJ (1989) Two-site/two-region models for pesticide transport and degradation: theoretical development and analytical solutions. Soil Sci Soc Am J 53(5):1303–1310. https://doi.org/10.2136/sssaj1989.03615995005300050001x

Wang D, Li C, Parikh SJ, Scow KM (2019a) Impact of biochar on water retention of two agricultural soils – a multi-scale analysis. Geoderma 340:185–191. https://doi.org/10.1016/j.geoderma.2019.01.012

Wang Y, Zhang W, Shang J, Shen C, Joseph SD (2019b) Chemical aging changed aggregation kinetics and transport of biochar colloids. Environ Sci Technol 53(14):8136–8146. https://doi.org/10.1021/acs.est.9b00583

Wang L, O'Connor D, Rinklebe J, Ok YS, Tsang DCW, Shen Z, Hou D (2020) Biochar aging: mechanisms, physicochemical changes, assessment, and implications for field applications. Environ Sci Technol 54:14797–14814. https://doi.org/10.1021/acs.est.0c04033

Wei J, Liu Y, Li J, Zhu Y, Yu H, Peng Y (2019) Adsorption and co-adsorption of tetracycline and doxycycline by one-step synthesized iron loaded sludge biochar. Chemosphere 236:124254. https://doi.org/10.1016/j.chemosphere.2019.06.224

Yang F, Zhao L, Gao B, Xu X, Cao X (2016) The interfacial behavior between biochar and soil minerals and its effect on biochar stability. Environ Sci Technol 50(5):2264–2271. https://doi.org/10.1021/acs.est.5b03656

Yi Q, Liang B, Nan Q, Wang H, Zhang W, Wu W (2020) Temporal physicochemical changes and transformation of biochar in a rice paddy: Insights from a 9-year field experiment. Sci Total Environ 721:137670. https://doi.org/10.1016/j.scitotenv.2020.137670

Yin WM, Guan Z, Liu C, He Y, Yang F, Tang XY (2019) Effects of biochar application and ageing on the adsorption of antibiotics in purple soil. Environ Sci 40(6):2920–2929. https://doi.org/10.13227/j.hjkx.201811141

Zhou D, Thiele-Bruhn S, Arenz-Leufen MG, Jacques D, Lichtner P, Engelhardt I (2016) Impact of manure-related DOM on sulfonamide transport in arable soils. J Contam Hydrol 192:118–128. https://doi.org/10.1016/j.jconhyd.2016.07.005

Zhuang L, Raoof A, Mahmoodlu MG, Biekart S, de Witte R, Badi L, Van Genuchten MT, Lin K (2021) Unsaturated flow effects on solute transport in porous media. J Hydrol 598:126301. https://doi.org/10.1016/j.jhydrol.2021.126301

Zimmerman AR (2010) Abiotic and microbial oxidation of laboratory-produced black carbon (biochar). Environ Sci Technol 44(4):1295–1301. https://doi.org/10.1021/es903140c

Zou Y, Zheng W (2013) Modeling manure colloid-facilitated transport of the weakly hydrophobic antibiotic florfenicol in saturated soil columns. Environ Sci Technol 47(10):5185–5192. https://doi.org/10.1021/es400624w